Variable kinematic beam elements coupled via Arlequin method

Variable kinematic beam elements coupled via Arlequin method F.

Biscani [a,b,c], G. Giunta [a,*], S. Belouettar [a], E. Carrera [b], H . H u [d]

a Centre de Recherche Public Henri Tudor, 29, av. John F. Kennedy, L-1855 Luxembourg-Kirchberg, Luxembourg
b Politecnico di Torino, 24, c.so Duca degli Abruzzi, 10129 Turin, Italy
c Institut Jean le Rond d'Alembert, UMR 7190, CNRS UNIV Paris 06, Case 162, Tour 55-65, 4, Place Jussieu, 75252 Paris, France
d School of Civil Engineering, Wuhan University, 8, South Road of East Lake, Wuchang, 430072 Wuhan, PR China

1. Introduction

Beam structures are widely used in many industrial fields. Helicopter rotor blades in aerospace engineering and concrete made beams in civil engineering represent just two examples. In order to achieve an effective design, the mechanics of beam structures should be modelled as accurate as possible, especially in the case of non-trivial cross sections or composite materials. The drawback of refined beam theories or three-dimensional analyses is represented by the computational cost. This work proposes a compromise between these opposite drivers. Via the Arlequin method, a refined beam model is adopted only for specific portions of the beam, whereas the remaining parts are modelled through a low-order theory. A brief discussion on refined beam formulation and computational techniques to combine different domains follows. In the case of bending mechanics, classical one-dimensional models are represented by Euler–Bernoulli's (EB) and Timoshenko's (TB) theories (see Timoshenko [1,2]). The cross-section is considered to be rigid on its plane. EB discards the shear deformation while TB accounts for a constant value. In the case of torsion, Saint-Venant's [3] and Prandtl's [4] models are the classical solutions. Classical theories do not yield accurate results in the case of unconventional cross-section geometries, short beams, anisotropic materials and non-homogeneous sections. In these contexts, refined theories are necessary. Improvements in classical models have been proposed to account for non-classical effects and non-conventional materials. A general review on beam modelling was proposed by Kapania and Raciti [5,6] accounting for static, buckling, free-vibration and wave propagation analysis. Other reviews are the ones by Hodges [7] and Jung et al. [8]. A unified formulation (UF) of axiomatically refined beam models was proposed by Carrera et Giunta [9]. Displacement-based theories accounting for non-classical effects (such as transverse shear and cross-section in- and out-of-plane warping) were derived. EB and TB models were retrieved as particular cases. Through a concise notation for the displacement field, problem gov-erning equations were reduced to a 'fundamental nucleo' that does not depend upon the approximation order, which is a free parame-ter of the formulation. The corresponding hierarchical finite ele-ments were addressed by Carrera et al. [10].

As far as coupling of "refined" and "coarse" sub-domains of a structure is concerned, several numerical methods have been formulated in the last years. In such a manner accurate results can be obtained with a reduced computational cost. In the sequential adaptation methods, structure's sub-domains differ in mesh size (*h*-adaptation, see Bank [11]) or degrees of freedom of the shape

functions (*p*-adaptation, see Szabo and Babuska [12]) or both (*hp*-adaptation, see Bathe [13]). Mesh size and shape functions are mod-ified according to a sequential approach based on the iteration of analysis and error estimation. In the multi-grid method (see Fish et al. [14]), coarse and fine meshes share information inside an iterative algorithm. In the extended finite element method by Möes [15], the basis of the shape functions is enriched to account for the discontinuity of the displacement field. The previous methods can be addressed as mono-model methods. In the case of multi-models methods, structure's sub-domains differ in the kinematic assumptions, that is, the very numerical models are adapted. In the *s*-version method (see Fish [16] and Fish and Markolefas [17]), incompatible meshes (different element size and polynomial order) with a local-global border are coupled. A variational approach to couple kinematically incompatible structural models was presented by Blanco et al. [18]. Ben Dhia et al. [19–21] proposed the Arlequin method. The coupling among different numerical models is obtained through Lagrange multipliers. This method was adopted by Hu et al.[22,23] for the linear and non-linear analysis of sandwich beams modelled via one- and two-dimensional finite elements. In the pres-ent work, the Arlequin method is formulated in the context of the beam unified approach by Carrera and Giunta [9]. Among the sub-domains to be coupled, the finite elements differ by the approxima-tion order of the displacement field, being the scale of the element the same. High-order elements are employed in the portion of the structure in which low-order theories would yield inaccurate re-sults, i.e. where the stress field is quasi-three-dimensional. Slender, moderately deep and deep beams are investigated. Square and I-shaped sections are considered. Isotropic or laminated composite materials are accounted for. The proposed approach is validated to-wards Navier-type analytical solutions and three-dimensional FEM models. Accurate results have been obtained with a significant reduction of the degrees of freedom of the models.

2. Preliminaries

A beam is a structure whose axial extension (l) is predominant with respect to any other dimension orthogonal to it. The cross-section (Ω) is defined by intersecting the beam with planes orthogonal to its axis. A Cartesian reference system is adopted. The x coordinate is coincident to the axis of the beam and it is bounded such that $0 \leqslant x \leqslant l$, y- and z-axis are two orthogonal directions laying on Ω. The cross-section is considered to be constant along x. The displacement field is:

$$\mathbf{u}^T(x,y,z) = \{\, u_x(x,y,z) \quad u_y(x,y,z) \quad u_z(x,y,z) \,\} \tag{1}$$

in which u_x, u_y and u_z are the displacement components along x-, y- and z-axes. Superscript 'T' represents the transposition operator. Stress ($\boldsymbol{\sigma}$) and strain ($\boldsymbol{\varepsilon}$) vectors are grouped into vectors $\boldsymbol{\sigma}_n$, $\boldsymbol{\varepsilon}_n$ acting on the cross-section:

$$\boldsymbol{\sigma}_n^T = \{\, \sigma_{xx} \quad \sigma_{xy} \quad \sigma_{xz} \,\} \quad \boldsymbol{\varepsilon}_n^T = \{\, \varepsilon_{xx} \quad \gamma_{xy} \quad \gamma_{xz} \,\} \tag{2}$$

and $\boldsymbol{\sigma}_p$, $\boldsymbol{\varepsilon}_p$ acting on planes orthogonal to Ω:

$$\boldsymbol{\sigma}_p^T = \{\, \sigma_{yy} \quad \sigma_{zz} \quad \sigma_{yz} \,\} \quad \boldsymbol{\varepsilon}_p^T = \{\, \varepsilon_{yy} \quad \varepsilon_{zz} \quad \gamma_{yz} \,\} \tag{3}$$

In the case of small displacements, linear relations between strains and displacements hold:

$$\boldsymbol{\varepsilon}_n^T = \{\, u_{x,x} \quad u_{x,y} + u_{y,x} \quad u_{x,z} + u_{z,x} \,\} \quad \boldsymbol{\varepsilon}_p^T = \{\, u_{y,y} \quad u_{z,z} \quad u_{y,z} + u_{z,y} \,\} \tag{4}$$

Subscripts 'x', 'y' and 'z', when preceded by comma, represent deri-vation versus the corresponding spatial coordinate. Eq. (4) in a com-pact vectorial notation read:

$$\boldsymbol{\varepsilon}_n = \mathbf{D}_{np}\mathbf{u} + \mathbf{D}_{nx}\mathbf{u} \quad \boldsymbol{\varepsilon}_p = \mathbf{D}_p\mathbf{u} \tag{5}$$

$\mathbf{D}_{np}$, $\mathbf{D}_{nx}$, and $\mathbf{D}_p$ are the following differential matrix operators:

$$\mathbf{D}_{np} = \begin{bmatrix} 0 & 0 & 0 \\ \frac{\partial}{\partial y} & 0 & 0 \\ \frac{\partial}{\partial z} & 0 & 0 \end{bmatrix} \quad \mathbf{D}_{nx} = \mathbf{I}\frac{\partial}{\partial x} \quad \mathbf{D}_p = \begin{bmatrix} 0 & \frac{\partial}{\partial y} & 0 \\ 0 & 0 & \frac{\partial}{\partial z} \\ 0 & \frac{\partial}{\partial z} & \frac{\partial}{\partial y} \end{bmatrix} \tag{6}$$

$\mathbf{I}$ is the unit matrix. Under the hypothesis of linear elastic materials, the generalised Hooke law holds. According to Eqs. (2) and (3), it reads:

$$\begin{aligned} \boldsymbol{\sigma}_p &= \widetilde{\mathbf{C}}_{pp}\boldsymbol{\varepsilon}_p + \widetilde{\mathbf{C}}_{pn}\boldsymbol{\varepsilon}_n \\ \boldsymbol{\sigma}_n &= \widetilde{\mathbf{C}}_{np}\boldsymbol{\varepsilon}_p + \widetilde{\mathbf{C}}_{nn}\boldsymbol{\varepsilon}_n \end{aligned} \tag{7}$$

In the case of fibres laying on planes parallel to the x-y one, matrices $\widetilde{\mathbf{C}}_{pp}$, $\widetilde{\mathbf{C}}_{pn}$, $\widetilde{\mathbf{C}}_{np}$ and $\widetilde{\mathbf{C}}_{nn}$ are:

$$\begin{aligned} \widetilde{\mathbf{C}}_{pp} &= \begin{bmatrix} \widetilde{C}_{22} & \widetilde{C}_{23} & 0 \\ \widetilde{C}_{23} & \widetilde{C}_{33} & 0 \\ 0 & 0 & \widetilde{C}_{44} \end{bmatrix} \quad \widetilde{\mathbf{C}}_{pn} = \widetilde{\mathbf{C}}_{np}^T = \begin{bmatrix} \widetilde{C}_{12} & \widetilde{C}_{26} & 0 \\ \widetilde{C}_{13} & \widetilde{C}_{36} & 0 \\ 0 & 0 & \widetilde{C}_{45} \end{bmatrix} \\ \widetilde{\mathbf{C}}_{nn} &= \begin{bmatrix} \widetilde{C}_{11} & \widetilde{C}_{16} & 0 \\ \widetilde{C}_{16} & \widetilde{C}_{66} & 0 \\ 0 & 0 & \widetilde{C}_{55} \end{bmatrix} \end{aligned} \tag{8}$$

For sake of brevity, coefficients $\widetilde{C}_{ij}$ in Eq. (8) are not reported here. They can be found as function of the engineering material constants and fibre rotation angle measured versus x-axis in Reddy [24]. In the case of classical models, the material stiffness coefficients should be corrected in order to contrast a phenomenon known in literature as Poisson's locking (see Carrera and Brischetto [25,26]). Poisson's ratio couples the normal deformations along the spatial directions. Because of this, a constant approximation of the displacement components u_y and u_z does not yield accurate results, even in the case of slender beams. A modified version of material's constitutive equations, in which the stiffness coefficients are opportunely modified, is obtained imposing σ_{yy} and σ_{zz} equal to zero in Hooke's law. An algebraic linear system in ε_{yy} and ε_{zz} is obtained. By substituting its solution into Hooke's equations regarding σ_{xx} and σ_{xy} the re-duced stiffness coefficients $\widetilde{Q}_{11}$, $\widetilde{Q}_{16}$ and $\widetilde{Q}_{66}$ are obtained:

$$\begin{aligned} \widetilde{Q}_{11} &= \widetilde{C}_{11} + \widetilde{C}_{12}\frac{\widetilde{C}_{12}\widetilde{C}_{33} - \widetilde{C}_{13}\widetilde{C}_{23}}{\widetilde{C}_{23}^2 - \widetilde{C}_{22}\widetilde{C}_{33}} + \widetilde{C}_{13}\frac{\widetilde{C}_{22}\widetilde{C}_{13} - \widetilde{C}_{12}\widetilde{C}_{23}}{\widetilde{C}_{23}^2 - \widetilde{C}_{22}\widetilde{C}_{33}} \\ \widetilde{Q}_{16} &= \widetilde{C}_{16} + \widetilde{C}_{26}\frac{\widetilde{C}_{12}\widetilde{C}_{33} - \widetilde{C}_{13}\widetilde{C}_{23}}{\widetilde{C}_{23}^2 - \widetilde{C}_{22}\widetilde{C}_{33}} + \widetilde{C}_{36}\frac{\widetilde{C}_{22}\widetilde{C}_{13} - \widetilde{C}_{12}\widetilde{C}_{23}}{\widetilde{C}_{23}^2 - \widetilde{C}_{22}\widetilde{C}_{33}} \\ \widetilde{Q}_{66} &= \widetilde{C}_{66} + \widetilde{C}_{26}\frac{\widetilde{C}_{26}\widetilde{C}_{33} - \widetilde{C}_{36}\widetilde{C}_{23}}{\widetilde{C}_{23}^2 - \widetilde{C}_{22}\widetilde{C}_{33}} + \widetilde{C}_{36}\frac{\widetilde{C}_{22}\widetilde{C}_{36} - \widetilde{C}_{26}\widetilde{C}_{23}}{\widetilde{C}_{23}^2 - \widetilde{C}_{22}\widetilde{C}_{33}} \end{aligned} \tag{9}$$

The new constitutive relations in the case of TB read:

$$\begin{aligned} \sigma_{xx} &= \widetilde{Q}_{11}\varepsilon_{xx} + \widetilde{Q}_{16}\gamma_{xy} \\ \sigma_{xy} &= \widetilde{Q}_{16}\varepsilon_{xx} + \widetilde{Q}_{66}\gamma_{xy} \\ \sigma_{xz} &= \widetilde{C}_{55}\gamma_{xz} \quad \sigma_{yz} = \widetilde{C}_{45}\gamma_{xz} \end{aligned} \tag{10}$$

whereas for EB, they reduce to the following equation:

$$\sigma_{xx} = \widetilde{Q}_{11}\varepsilon_{xx} \tag{11}$$

3. Hierarchical beam theories

Hierarchical displacement-based theories can be formulated on the basis of the following generic kinematic field:

$$\mathbf{u}(x,y,z) = F_\tau(y,z)\mathbf{u}_\tau(x) \quad \text{with } \tau = 1,2,\ldots,N_u \tag{12}$$

where N_u stands for the number of unknowns and depends on the approximation order N. This latter is a free parameter of the formulation. On the basis of Einstein's notation, subscript τ is a dummy index that indicates summation over the range $[1,N_u]$. Thanks to

this notation, problem's governing differential equations and boundary conditions are derived in terms of a single 'fundamental nucleo'. The theoretical formulation is valid for a generic approximation order and approximating functions $F_\tau(y,z)$. In this paper, the functions F_τ are assumed to be Mac Laurin's polynomials. N_u and F_τ as functions of N can be obtained via Pascal's triangle (see Ta-ble 1). The actual governing differential equations and boundary conditions due to a fixed approximation order are obtained straightforwardly via summation of the nucleo corresponding to each term of the expansion. According to the previous choice of polynomial function, the generic N-order displacement field is:

$$\begin{aligned} u_x &= u_{x1} + u_{x2}y + u_{x3}z + \cdots + u_{x\frac{(N^2+N+2)}{2}}y^N + \cdots + u_{x\frac{(N+1)(N+2)}{2}}z^N \\ u_y &= u_{y1} + u_{y2}y + u_{y3}z + \cdots + u_{y\frac{(N^2+N+2)}{2}}y^N + \cdots + u_{y\frac{(N+1)(N+2)}{2}}z^N \\ u_z &= u_{z1} + u_{z2}y + u_{z3}z + \cdots + u_{z\frac{(N^2+N+2)}{2}}y^N + \cdots + u_{z\frac{(N+1)(N+2)}{2}}z^N \end{aligned} \tag{13}$$

As far as the first-order approximation order is concerned, the kinematic field is:

$$\begin{aligned} u_x &= u_{x1} + u_{x2}y + u_{x3}z \\ u_y &= u_{y1} + u_{y2}y + u_{y3}z \\ u_z &= u_{z1} + u_{z2}y + u_{z3}z \end{aligned} \tag{14}$$

Classical models, such as TB:

$$\begin{aligned} u_x &= u_{x1} + u_{x2}y + u_{x3}z \\ u_y &= u_{y1} \\ u_z &= u_{z1} \end{aligned} \tag{15}$$

and EB:

$$\begin{aligned} u_x &= u_{x1} - u_{y1,x}y - u_{z1,x}z \\ u_y &= u_{y1} \\ u_z &= u_{z1} \end{aligned} \tag{16}$$

are straightforwardly derived from the first-order approximation model. Higher order models yield a more detailed description of the shear mechanics (no shear correction coefficient is required), of the in- and out-of-section deformations, of the coupling between the spatial directions due to Poisson's effect and of the torsional mechanics than classical models do. EB theory neglects them all, since it was formulated to describe the bending mechanics. TB model accounts for constant shear stress and strain components.

4. Finite element formulation

In the framework of the finite element modelling, the displacement vector is approximated as:

$$\mathbf{u} = N_i F_\tau \mathbf{q}_{\tau i} \tag{17}$$

where $\mathbf{q}_{\tau i}$ is the nodal displacement vector:

$$\mathbf{q}_{\tau i}^T = \left\{ q_{u_{x\tau i}} \;\; q_{u_{y\tau i}} \;\; q_{u_{z\tau i}} \right\} \tag{18}$$

and N_i are the shape functions as in Bathe [13]. Dummy index i ranger over the element nodes. Elements with two, three and four nodes are considered. Through the paper they are addressed as B2, B3 and B4, respectively. Elements' stiffness matrix and external loadings vector are obtained through the Principle of Virtual Displacements (PVD):

$$\delta L^{int} = \delta L^{ext} \tag{19}$$

δstands for a virtual variation. L^{ext} stands for the work due to external loadings. L^{int} represents the strain energy. According to the grouping of the stress and strain components in Eqs. (2) and (3), it can be written as the sum of two contributes:

$$\delta L^{int} = \int_l \int_\Omega \left(\delta \boldsymbol{\epsilon}_n^T \boldsymbol{\sigma}_n + \delta \boldsymbol{\epsilon}_p^T \boldsymbol{\sigma}_p \right) d\Omega dx \tag{20}$$

Via substitution of Eqs. (5), (7) and (17), (20) reads:

$$\begin{aligned} \delta L^{int} = \int_l \int_\Omega \delta \mathbf{q}_{sj}^T \Big[& N_i \left(\mathbf{D}_{nx}^T N_j \right) \widetilde{\mathbf{C}}_{np} F_s (\mathbf{D}_p F_\tau) + F_s F_\tau \left(\mathbf{D}_{nx}^T N_j \right) \widetilde{\mathbf{C}}_{nn} (\mathbf{D}_{nx} N_i) \\ & + N_i \left(\mathbf{D}_{nx}^T N_j \right) \widetilde{\mathbf{C}}_{nn} F_s (\mathbf{D}_{np} F_\tau) + N_i N_j \left(\mathbf{D}_{np}^T F_s \right) \widetilde{\mathbf{C}}_{np} (\mathbf{D}_p F_\tau) \\ & + F_\tau \left(\mathbf{D}_{np}^T F_s \right) \widetilde{\mathbf{C}}_{nn} N_j (\mathbf{D}_{nx} N_i) + N_i N_j \left(\mathbf{D}_{np}^T F_s \right) \widetilde{\mathbf{C}}_{nn} (\mathbf{D}_{np} F_\tau) \\ & + N_i N_j \left(\mathbf{D}_p^T F_s \right) \widetilde{\mathbf{C}}_{pp} (\mathbf{D}_p F_\tau) + F_\tau \left(\mathbf{D}_p^T F_s \right) \widetilde{\mathbf{C}}_{pn} N_j (\mathbf{D}_{nx} N_i) \\ & + N_i N_j \left(\mathbf{D}_p^T F_s \right) \widetilde{\mathbf{C}}_{pn} (\mathbf{D}_{np} F_\tau) \Big] \mathbf{q}_{\tau i} d\Omega dx \end{aligned} \tag{21}$$

Indexes i and j range over the number of nodes of the element, whereas τ, s are related to the expansion functions. Eq. (21) can be rewritten in a compact form as:

$$\delta L^{int} = \delta \mathbf{q}_{sj}^T \mathbf{K}^{ij\tau s} \mathbf{q}_{\tau i} \tag{22}$$

where $\mathbf{K}^{ij\tau s}$ is the fundamental nucleo of the stiffness matrix. Its components are:

$$\begin{aligned} K_{xx}^{ij\tau s} &= I_{i,xj,x} J_{\tau s}^{11} + I_{ij,x} J_{\tau,ys}^{16} + I_{i,xj} J_{\tau s,y}^{16} + I_{ij} \left(J_{\tau,ys,y}^{66} + J_{\tau,zs,z}^{66} \right) \\ K_{xy}^{ij\tau s} &= I_{i,xj,x} J_{\tau s}^{16} + I_{ij,x} J_{\tau,ys}^{12} + I_{i,xj} J_{\tau s,y}^{66} + I_{ij} \left(J_{\tau,ys,y}^{26} + J_{\tau,zs,z}^{45} \right) \\ K_{xz}^{ij\tau s} &= I_{ij,x} J_{\tau,zs}^{13} + I_{i,xj} J_{\tau s,z}^{55} + I_{ij} \left(J_{\tau,zs,y}^{36} + J_{\tau,ys,z}^{45} \right) \\ K_{xy}^{ij\tau s} &= I_{i,xj,x} J_{\tau s}^{16} + I_{ij,x} J_{\tau,ys}^{66} + I_{i,xj} J_{\tau s,y}^{12} + I_{ij} \left(J_{\tau,ys,y}^{26} + J_{\tau,zs,z}^{45} \right) \\ K_{yy}^{ij\tau s} &= I_{i,xj,x} J_{\tau s}^{66} + I_{ij,x} J_{\tau,ys}^{26} + I_{i,xj} J_{\tau s,y}^{26} + I_{ij} \left(J_{\tau,ys,y}^{22} + J_{\tau,zs,z}^{44} \right) \\ K_{yz}^{ij\tau s} &= I_{ij,x} J_{\tau,zs}^{36} + I_{i,xj} J_{\tau s,z}^{45} + I_{ij} \left(J_{\tau,zs,y}^{23} + J_{\tau,ys,z}^{44} \right) \\ K_{zx}^{ij\tau s} &= I_{ij,x} J_{\tau,zs}^{55} + I_{i,xj} J_{\tau s,z}^{13} + I_{ij} \left(J_{\tau,zs,y}^{45} + J_{\tau,ys,z}^{36} \right) \\ K_{zy}^{ij\tau s} &= I_{ij,x} J_{\tau,zs}^{45} + I_{i,xj} J_{\tau s,z}^{36} + I_{ij} \left(J_{\tau,zs,y}^{44} + J_{\tau,ys,z}^{23} \right) \\ K_{zz}^{ij\tau s} &= I_{i,xj,x} J_{\tau s}^{55} + I_{ij,x} J_{\tau,ys}^{45} + I_{i,xj} J_{\tau s,y}^{45} + I_{ij} \left(J_{\tau,ys,y}^{44} + J_{\tau,zs,z}^{33} \right) \end{aligned} \tag{23}$$

where

$$I_{i_{(x)}j_{(x)}} = \int_l N_{i_{(x)}} N_{j_{(x)}} \, dx \tag{24}$$

and

$$J_{\tau_{(y)(z)}s_{(y)(z)}}^{mn} = \int_\Omega \widetilde{C}_{mn} F_{\tau_{(y)(z)}} F_{s_{(y)(z)}} \, d\Omega \tag{25}$$

As far as the whole structure is concerned, the constant kinematic FEM problem in the framework of the proposed unified formulation is governed by the following equation:

$$\overline{\mathbf{K}}^{ij\tau s} \bar{\mathbf{q}}_{\tau i} = \overline{\mathbf{P}}_{sj} \tag{26}$$

where $\overline{\mathbf{K}}^{ij\tau s}$ and $\bar{\mathbf{q}}_{\tau i}$ are the global stiffness matrix and nodal displacement vector. $\overline{\mathbf{P}}_{si}$ is a loading vector that is variationally coherent to the mechanical model through the external work.

Table 1
Mac Laurin's polynomials via Pascal's triangle.

N	N_u	F_τ
0	1	$F_1 = 1$
1	3	$F_2 = y$ $F_3 = z$
2	6	$F_4 = y^2$ $F_5 = yz$ $F_6 = z^2$
3	10	$F_7 = y^3$ $F_8 = y^2 z$ $F_9 = yz^2$ $F_{10} = z^3$
...	...	...
N	$\frac{(N+1)(N+2)}{2}$	$F_{\frac{(N^2+N+2)}{2}} = y^N$ $F_{\frac{(N^2+N+4)}{2}} = y^{N-1}z \cdots F_{\frac{N(N+3)}{2}} = yz^{N-1}$ $F_{\frac{(N+1)(N+2)}{2}} = z^N$

5. Arlequin method in the context of hierarchical beam theories

The beam volume (V) is axially divided into two sub-domains A_1 and A_2 that are partially overlapped, see Fig. 1. S represents the overlapping volume. For each sub-domain, a different expansion order is assumed:

$$\mathbf{u}_\xi = N_i F_{\tau_\xi} \mathbf{q}_{\tau_\xi i} \quad \text{with } \tau_\xi = 1,2,\dots,N_u^{A_\xi}, \quad \xi = 1,2 \tag{27}$$

being ξ a dummy index that counts the sub-domains. The global mechanical problem is solved by merging together the two sub-domains via the Arlequin method. The internal and external virtual works are computed for each sub-domain. The structural integrity in the overlapping volume is ensured via a Lagrangian multiplier field ($\boldsymbol{\lambda}$) and a coupling operator (C_ξ) that links the degrees of freedom of each sub-domain within the overlapping volume. The PVD becomes:

$$\delta L_\xi^{int}(\mathbf{u}_\xi) + \delta L_\xi^{c}(\mathbf{u}_\xi) = \delta L_\xi^{ext} \tag{28}$$

The virtual variation of the strain energy in each sub-domain is:

$$\delta L_\xi^{int} = \int_{A_\xi} \alpha_\xi \left(\delta \boldsymbol{\epsilon}_n^T \boldsymbol{\sigma}_n + \delta \boldsymbol{\epsilon}_p^T \boldsymbol{\sigma}_p \right) dV \quad \text{with} \begin{cases} \alpha_\xi = 1 & \text{in } A_\xi \setminus S \\ \alpha_1 + \alpha_2 = 1 & \text{in } S \end{cases} \tag{29}$$

$\alpha_\xi$are weighting functions for scaling the energy in each sub-domain in order to not consider the energy in the overlapping volume twice. According to Ben Dhia [20], they should be such that the sub-domain with a more accurate description has a higher weight in the global equilibrium. Unless differently stated, a constant value equal to 0.99 is assumed for the sub-domain in which the refined model is adopted. The virtual external work is treated in a similar manner. δL_ξ^c is the virtual coupling work:

$$\delta L_\xi^c = (-1)^\xi C_\xi(\delta\boldsymbol{\lambda}, \mathbf{u}_\xi) \tag{30}$$

Two coupling operators are considered (see Hu et al. [22]):

- L^2 coupling:

$$\delta C_\xi = \int_{S_\xi} \delta\boldsymbol{\lambda}^T \mathbf{u}_\xi dV \tag{31}$$

- H^1 coupling:

$$\delta C_\xi = \int_{S_\xi} \left\{ \delta\boldsymbol{\lambda}^T \mathbf{u}_\xi + \tilde{l}^2 \left[\delta\boldsymbol{\varepsilon}_n^T(\boldsymbol{\lambda}) \boldsymbol{\varepsilon}_n(\mathbf{u}_\xi) + \delta\boldsymbol{\varepsilon}_p^T(\boldsymbol{\lambda}) \boldsymbol{\varepsilon}_p(\mathbf{u}_\xi) \right] \right\} dV \tag{32}$$

$\tilde{l}$ is a real parameter representative of a characteristic length. $\boldsymbol{\varepsilon}(\boldsymbol{\lambda})$ is defined in the same manner as the mechanical strain $\boldsymbol{\varepsilon}(\mathbf{u}_\xi)$, where the Lagrangian multiplier field is used instead of the displacement one. The Lagrangian multiplier is discretised according to the UF:

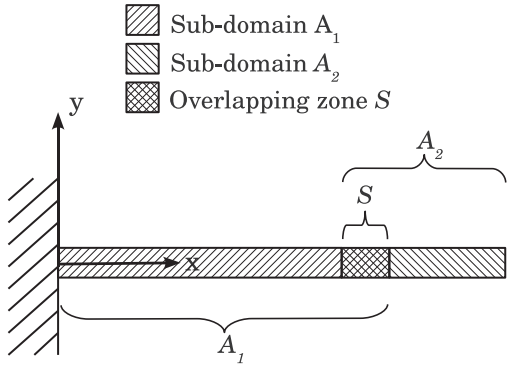

Fig. 1. Beam structure divided into two overlapping sub-domains.

$$\boldsymbol{\lambda} = N_i F_{\tau_\lambda} \boldsymbol{\Lambda}_{\tau_\lambda i} \tag{33}$$

where $\boldsymbol{\Lambda}_{\tau_\lambda i}$ is the nodal unknown vector. The fundamental nucleo of the coupling matrix $\mathbf{C}_\xi^{ij\tau_\xi s_\lambda}$ is derived coherently to Eq. (22) via substitution of Eq. (33) into Eq. (31) or (32):

$$\delta C_\xi = \delta \boldsymbol{\Lambda}_{s_\lambda j}^T \mathbf{C}_\xi^{ij\tau_\xi s_\lambda} \mathbf{q}_{\tau_\xi i} \tag{34}$$

In the case of L^2 coupling, the fundamental nucleo is diagonal and its components are:

$$C_{\xi mn}^{ij\tau_\xi s_\lambda} = \delta_{nm} I_{ij} J_{\tau_\xi s_\lambda} \quad \text{with } m,n = x,y,z \tag{35}$$

where δ_{nm} is Kronecker's delta. Terms I_{ij} have been defined in Eq. (24) and:

$$J_{\tau_\xi s_\lambda} = \int_\Omega F_{\tau_\xi} F_{s_\lambda} d\Omega \tag{36}$$

For the coupling operator H^1, coupling matrix fundamental nucleo can be obtained straightforwardly noticing that H^1 coupling operator is the sum of the L^2 one and a term similar to the virtual internal work in Eq. (20). The components of this latter term are those of the stiffness matrix that correspond to the diagonal terms of the constitutive matrices $\tilde{\mathbf{C}}_{pp}$ and $\tilde{\mathbf{C}}_{nn}$:

$$\begin{aligned}
&C_{\xi xx}^{ij\tau_\xi s_\lambda} = C_{\xi yy}^{ij\tau_\xi s_\lambda} = C_{\xi zz}^{ij\tau_\xi s_\lambda} = I_{ij} J_{\tau_\xi s_\lambda} + \tilde{l}^2 [I_{i,xj,x} J_{\tau_\xi s_\lambda} + I_{ij} (J_{\tau_\xi, y s_\lambda, y} + J_{\tau_\xi, z s_\lambda, z})] \\
&C_{\xi xy}^{ij\tau_\xi s_\lambda} = \tilde{l}^2 I_{i,xj} J_{\tau_\xi s_\lambda, y} \qquad C_{\xi yx}^{ij\tau_\xi s_\lambda} = \tilde{l}^2 I_{ij,x} J_{\tau_\xi, y s_\lambda} \\
&C_{\xi xz}^{ij\tau_\xi s_\lambda} = \tilde{l}^2 I_{i,xj} J_{\tau_\xi s_\lambda, z} \qquad C_{\xi zx}^{ij\tau_\xi s_\lambda} = \tilde{l}^2 I_{ij,x} J_{\tau_\xi, z s_\lambda} \\
&C_{\xi yz}^{ij\tau_\xi s_\lambda} = \tilde{l}^2 I_{ij} J_{\tau_\xi, y s_\lambda, z} \qquad C_{\xi zy}^{ij\tau_\xi s_\lambda} = \tilde{l}^2 I_{ij} J_{\tau_\xi, z s_\lambda, y}
\end{aligned} \tag{37}$$

where

$$J_{\tau_{\xi(,y)(,z)} s_{\lambda(,y)(,z)}} = \int_\Omega F_{\tau_{\xi(,y)(,z)}} F_{s_{\lambda(,y)(,z)}} \, d\Omega \tag{38}$$

As suggested by Ben Dhia [20], the same approximation order should be assumed for the less accurate assumed model and the Lagrangian multiplier. Considering the whole structure and assuming that the refined model is adopted in the sub-domain A_2 (see Fig. 1):

$$N_u^{A_2} \geqslant N_u^{A_1} \tag{39}$$

the governing equations of the variable kinematic problem in the framework of the proposed unified formulation coupled via the Arlequin method are:

$$\begin{bmatrix}
\overline{\mathbf{K}}_{A_1\setminus S}^{ij\tau_1 s_1} & \mathbf{0} & \mathbf{0} & \mathbf{0} & \mathbf{0} \\
\mathbf{0} & (1-\alpha)\overline{\mathbf{K}}_{A_1\cap S}^{ij\tau_1 s_1} & \mathbf{0} & \mathbf{0} & \overline{\mathbf{C}}_1^{ij\tau_1 s_1 T} \\
\mathbf{0} & \mathbf{0} & \overline{\mathbf{K}}_{A_2\setminus S}^{ij\tau_2 s_2} & \mathbf{0} & \mathbf{0} \\
\mathbf{0} & \mathbf{0} & \mathbf{0} & \alpha\overline{\mathbf{K}}_{A_2\cap S}^{ij\tau_2 s_2} & -\overline{\mathbf{C}}_2^{ij\tau_2 s_1 T} \\
\mathbf{0} & \overline{\mathbf{C}}_1^{ij\tau_1 s_1} & \mathbf{0} & -\overline{\mathbf{C}}_2^{ij\tau_2 s_1} & \mathbf{0}
\end{bmatrix}
\begin{Bmatrix}
\bar{\mathbf{q}}_{\tau_1 i}^{A_1\setminus S} \\
\bar{\mathbf{q}}_{\tau_1 i}^{A_1\cap S} \\
\bar{\mathbf{q}}_{\tau_2 i}^{A_2\setminus S} \\
\bar{\mathbf{q}}_{\tau_2 i}^{A_2\cap S} \\
\overline{\boldsymbol{\Lambda}}_{\tau_1 i}
\end{Bmatrix}
=
\begin{Bmatrix}
\overline{\mathbf{P}}_{s_1 j}^{A_1\setminus S} \\
(1-\alpha)\overline{\mathbf{P}}_{s_1 j}^{A_1\cap S} \\
\overline{\mathbf{P}}_{s_2 j}^{A_2\setminus S} \\
\alpha\overline{\mathbf{P}}_{s_2 j}^{A_2\cap S} \\
0
\end{Bmatrix} \tag{40}$$

6. Numerical results and discussion

Analyses are carried out considering a square and a thin-walled I-shaped cross-section. In the latter, the wall thickness is equal to

10% of a main cross-section dimension a equal to 0.2 m. A cross-ply laminated composite beam is considered as well. Slender (l/a = 100), moderately deep (l/a = 30) and deep (l/a = 10) beams are accounted for. Beams are simply supported at both ends. They undergo a localised uniform pressure (P) equal to 1 Pa acting on 10%of the length and centred at mid-span. The loading is applied to the top of the cross-section, see Fig. 2. Out-of-plane displacement u_x and shear stress component σ_{xy} are evaluated at x = 0, whereas in-plane displacement components (u_y and u_z) and normal stresses (σ_{xx}, σ_{yy} and σ_{zz}) are computed at beam mid-span. For each cross-section, the proposed finite elements are first validated towards the corresponding closed form, Navier-type solution (see Carrera and Giunta [9]). For these latter, the localised loading is approxi-mated via a Fourier series expansion. The number of the approxi-mation terms is such that displacement and stress components converge up to three significant digits. Results are also validated towards three-dimensional FEM solutions obtained via the com-mercial code ABAQUS. For all the analyses, the quadratic C3DR20 element is used (see [27]). As far as a I-shaped cross-section is con-cerned, FEM models using plate elements are commonly consid-ered as reference solutions in literature. A three-dimensional FEM model has been here considered since plate elements avail-able on commercial FEM codes are generally based on classical Kir-chhoff's or Reissner's models and they do not yield the complete three-dimensional stress field. Meshes are such that the maximum displacement components converge up to four significant digits. After validation, elements based on a first- or second-order theory (low-order model) are coupled to those based on a fourth- or a 15th-order one (refined model) via the Arlequin method. Two configurations are considered. In the first one, addressed as "Arlequin^a", the refined sub-domain is near the loading application area. For the second configuration (Arlequin^b), the refined sub-do-main is near the constraint, see Fig. 2. These configurations have been addressed since load application regions and constrained re-gions are likely to present a three-dimensional stress field. In the general case in which the location of a three-dimensional stress field cannot be determined a priori, refined sub-domains should be chosen on the basis of experience and preliminary analyses via low-order models. Analyses have been carried out considering both L^2 and H^1 coupling. For this latter, different values of $\tilde{l}$ in Eq. (32) have been accounted for. In general, no relevant differences have been found. Unless differently stated, L^2 coupling is, therefore, used. Due to the symmetry of the problem, only half of the structure is investigated and only a superimposition volume is needed, see Fig. 2.

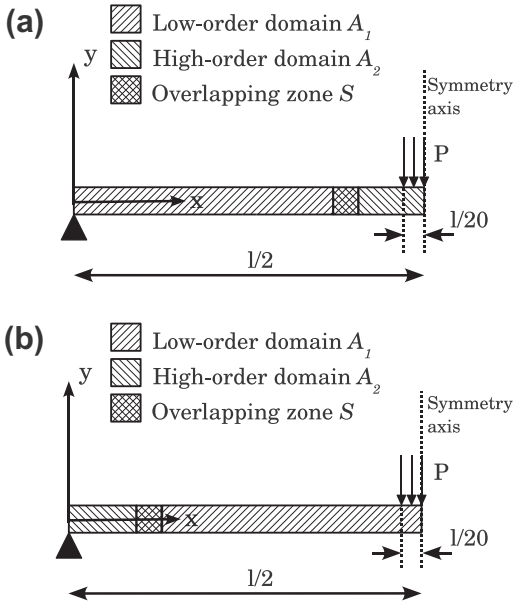

Fig. 2. Simply supported beams under a localised uniform pressure P. Arlequin model with refined elements near (a) the loading application zone or (b) the constraint.

6.1. Square cross-section beam

Cross-section geometry and loading are shown in Fig. 3. The figure presents also the points on the cross-section where displacements and stresses are evaluated. Beams are made of an isotropic material whose properties are: Young's modulus (E) equal to 75 GPa and Poisson's ratio (ν) equal to 0.3. Displacements and stresses are put in a dimensionless form as follows:

$$(\bar{u}_x, \bar{u}_y, \bar{u}_z) = \frac{4Ea}{l^2 P}(u_x, u_y, u_z) \tag{41}$$

$$(\bar{\sigma}_{xx}, \bar{\sigma}_{yy}, \bar{\sigma}_{xy}) = \frac{1}{P}(\sigma_{xx}, \sigma_{yy}, \sigma_{xy}) \tag{42}$$

Table 2 presents the displacement components for a slender beam. Results are computed considering 20 elements of the same length. Bending mechanics is predominant. Classical models, therefore, yield accurate results for $\bar{u}_x$ and $\bar{u}_y$. In order to predict correctly $\bar{u}_z$, a second-order theory is required. Finite element results con-verge to the analytical solution. Displacement components for the case of a deep beam are presented in Table 3. EB model underesti-mates $\bar{u}_y$ by about 1.2% since it does not account for shear effects. An accurate prediction of $\bar{u}_z$ calls for a second-order theory. Dimen-sionless stresses for slender and deep beams are reported in Tables 4 and 5, respectively. Stress component $\bar{\sigma}_{xx}$ converges to the analyt-ical solution regardless the number of nodes per element. In the case of $\bar{\sigma}_{xy}$ and $\bar{\sigma}_{yy}$, B2 and B3 elements call for a finer mesh. Con-vergence analysis is presented in Figs. 4 and 5 for slender and deep beams, respectively. A third-order model is considered. Ten ele-ments are sufficient in the case of B4 elements. Convergence for slender beams is slower than for deep ones. Classical theories cor-rectly predicts only $\bar{\sigma}_{xx}$. An accurate evaluation of $\bar{\sigma}_{xy}$ and $\bar{\sigma}_{yy}$ calls for at least a third-order theory. As far as a variable kinematic solu-tion is concerned, the coarse sub-domain A_1 is meshed via 16 first-order, B4 elements whereas five fourth-order, B4 elements are

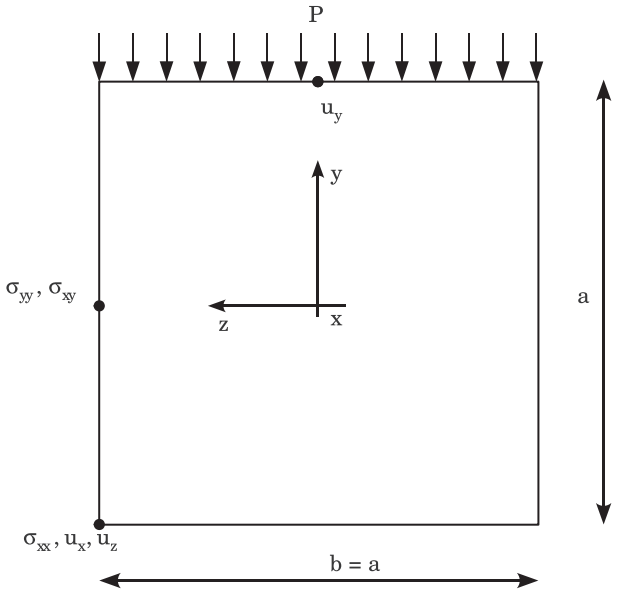

Fig. 3. Square cross-section geometry, loading and verification points.

Table 2
Dimensionless displacements for square cross-section beam, $l/a = 100$.

	$\bar{u}_x$			$10^{-2} \times \bar{u}_y$			$10^{2} \times \bar{u}_z$		
FEM 3D	3.737			2.488			2.125		
UF	B2	B3/4	AS [a]	B2	B3/4	AS	B2	B3/4	AS
$N = 3$	3.735	3.737	3.737	2.485	2.488	2.488	2.137	2.137	2.137
$N = 2$	3.735	3.737	3.737	2.485	2.488	2.488	2.137	2.137	2.137
$N = 1$	3.736	3.737	3.737	2.485	2.488	2.488	0.000	0.000	0.000
TB	3.735	3.737	3.737	2.485	2.488	2.488	0.000	0.000	0.000
EB	3.735	3.737	3.737	2.484	2.487	2.487	0.000	0.000	0.000

[a] Analytical UF solution.

Table 3
Dimensionless displacements for square cross-section beam, $l/a = 10$.

	$10^{1} \times \bar{u}_x$			$\bar{u}_y$			$10^{2} \times \bar{u}_z$		
FEM 3D	3.742			2.544			2.125		
UF	B2	B3/4	AS [a]	B2	B3/4	AS	B2	B3/4	AS
$N = 3$	3.740	3.741	3.741	2.541	2.544	2.544	2.111	2.113	2.113
$N = 2$	3.734	3.736	3.736	2.531	2.533	2.533	2.099	2.100	2.106
$N = 1$	3.747	3.749	3.749	2.549	2.522	2.522	−0.055	−0.053	−0.053
TB	3.735	3.737	3.737	2.546	2.549	2.549	0.000	0.000	0.000
EB	3.736	3.737	3.737	2.484	2.487	2.487	0.000	0.000	0.000

[a] Analytical UF solution.

Table 4
Dimensionless stresses in the case of beam with square cross-section, $l/a = 100$.

	$-10^{-3} \times \bar{\sigma}_{xx}$				$\bar{\sigma}_{xy}$				$10^{1} \times \bar{\sigma}_{yy}$			
FEM 3D	1.425				8.583				5.000			
UF	B2	B3	B4	AS[a]	B2	B3	B4	AS	B2	B3	B4	AS
$N = 4$	1.412	1.429	1.425	1.425	−27.59	20.48	8.461	8.461	0.806	4.141	5.578	5.000
$N = 3$	1.412	1.429	1.425	1.425	−27.59	20.48	8.461	8.461	0.722	4.088	5.552	4.997
$N = 1$	1.415	1.428	1.425	1.425	−31.05	17.01	5.000	5.000	2.367	4.349	5.074	5.242
TB	1.415	1.428	1.425	1.425	−31.05	17.01	5.000	5.000	–	–	–	–
EB	1.415	1.428	1.425	1.425	–	–	–	–	–	–	–	–

[a] Analytical UF solution.

Table 5
Dimensionless stresses in the case of beam with square cross-section, $l/a = 10$.

	$-10^{-1} \times \bar{\sigma}_{xx}$				$10^{1} \times \bar{\sigma}_{xy}$				$10^{1} \times \bar{\sigma}_{yy}$			
FEM 3D	1.428				8.595				5.278			
UF	B2	B3	B4	AS[a]	B2	B3	B4	AS	B2	B3	B4	AS
$N = 4$	1.410	1.427	1.425	1.425	8.100	8.581	8.461	8.462	6.015	5.192	5.214	5.208
$N = 3$	1.423	1.436	1.432	1.432	8.100	8.581	8.461	8.462	5.998	5.235	5.250	5.245
$N = 1$	1.437	1.450	1.446	1.446	4.639	5.120	5.000	5.000	5.020	4.865	4.870	4.871
TB	1.415	1.428	1.425	1.425	4.639	5.120	5.000	5.000	–	–	–	–
EB	1.415	1.428	1.425	1.425	–	–	–	–	–	–	–	–

[a] Analytical UF solution.

considered for sub-domain A_2. A superimposed element, whose length is l_{el}, is considered in the overlapping volume. Displacements and stresses for a deep beam are reported in Table 6. The total degrees of freedom (DOF) of each solution are also reported there. Results are aligned with those obtained through mono-theories models having the same expansion order, proving the effectiveness of the Arlequin method in coupling domains having finite elements based on theories with different expansion order. The case in which more than one superimposed element is present have been also investigated, but no significant difference has been found. In order to reduce the number of degrees of freedom, the best choice consists in only a superimposed element. A comparison between the considered variable kinematic models and the fourth-order mono-model shows that the total number of degrees of freedom is reduced by more than a half. Figs. 6–8 show the variation along the beam axis of u_y, u_z and σ_{yy}, respectively. Arlequin[a] solution is compared to a model with 20 fourth-order elements (named as "Reference"). In the overlapping volume S, two solutions exist. Their values do not necessarily match. Global bending response u_y is accurately described by both first- and fourth-order models. In the case of u_z, first-order theory does not account for the warping of the section, whereas fourth-order elements match the reference solution. In the case of σ_{yy}, both L^2 and H^1 coupling operators have been accounted for. In the case of H^1 coupling, the parameter $\tilde{l}$ is

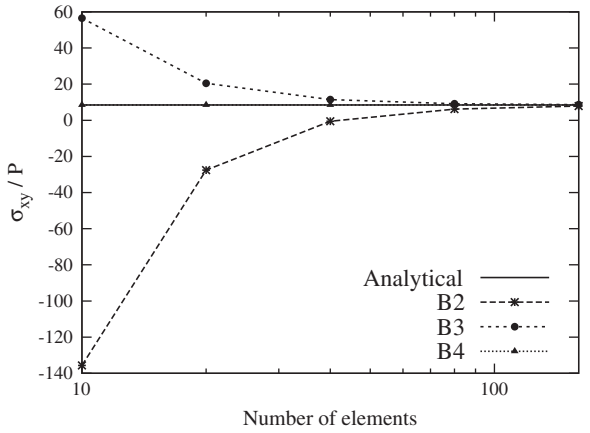

Fig. 4. Dimensionless stress $\bar{\sigma}_{xy}$ at $x = 0$ versus the number of elements for square cross-section beam, $l/a = 100$, third-order model.

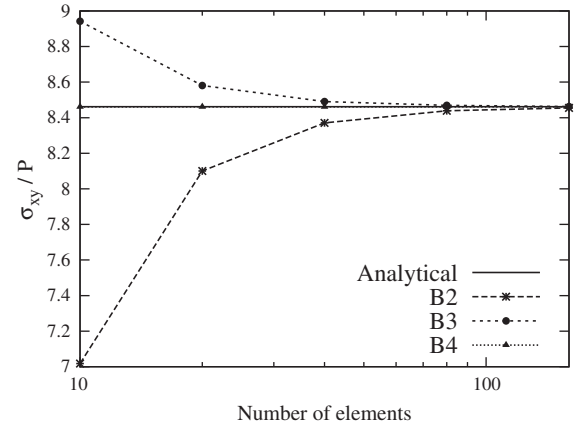

Fig. 5. Dimensionless stress $\bar{\sigma}_{xy}$ at $x = 0$ versus the number of elements for square cross-section beam, $l/a = 10$, third-order model.

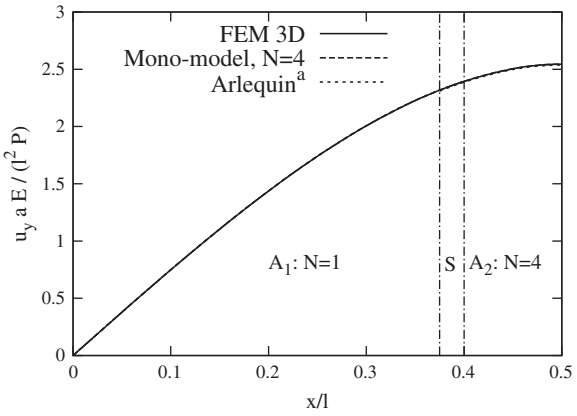

Fig. 6. Dimensionless displacement $\bar{u}_y$ along the beam axis for square cross-section, $l/a = 10$.

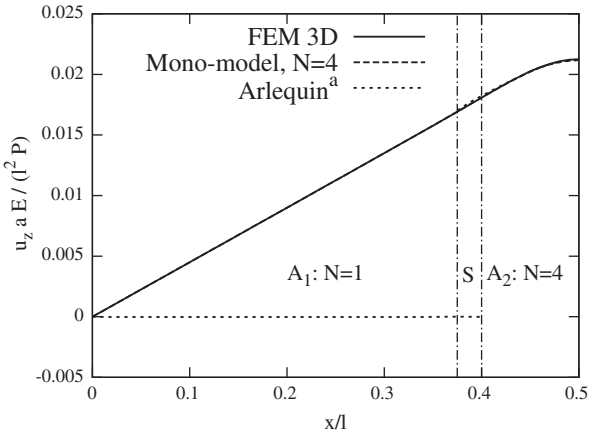

Fig. 7. Dimensionless displacement $\bar{u}_z$ along the beam axis for square cross-section, $l/a = 10$.

equal to l_{el}. Results differ slightly in the superimposed volume only. They do not change increasing $\tilde{l}$. H^1 solution converges to the L^2 one decreasing $\tilde{l}$. As far as the sensitivity of the Arlequin method upon the weighting functions α_ξ in Eq. (29) is concerned, Fig. 9 presents the influence of α_2 on σ_{yy}. α_2 influences the solution in the coupling domain. Increasing α_2, σ_{yy} becomes smoother and smoother since the refined model assumes more and more relevance. Outside the coupling domain, α_2 does not affect the solution. A qualitatively comparison of the stress component $\bar{}\sigma_{xy}$ via three-dimensional FEM solution, fourth-order model and Arlequin[b] solution is pre-sented in Fig. 10 in the form of colour maps above the cross-section. Results are in good agreement.

6.2. Laminated composite beam

A cross-ply laminated composite beam with a symmetric stacking sequence [0/90/0] is addressed. Fibres orientation is measured towards x-axis. Cross-section dimensions are such that $b/a \ll 1$, as shown in Fig. 11. Out-of-plane displacement u_z, transverse shear stress σ_{xz} and normal stress σ_{xx} are evaluated beam's top, centre and bottom, respectively. Layers are all made of the same material whose mechanical properties are: $E_L = 172$ GPa, $E_T = 6.9$ GPa, $G_{LT} = 3.5$ GPa, $G_{TT} = 1.4$ GPa, $\nu_{LT} = \nu_{TT} = 0.25$. '$L$' denotes a direction parallel to the fibres, whereas 'T' stands for a direction transverse to them. Beams undergo the same loading as in the previous case. Results are put in a dimensionless form as follows:

Table 6
Mono-theories and variable kinematic models, square cross-section beam, $l/a = 10$.

	$10^1 \times \bar{u}_x$	$\bar{u}_y$	$10^2 \times \bar{u}_z$	$-10^{-1} \times \bar{\sigma}_{xx}$	$10^1 \times \bar{\sigma}_{xy}$	$10^1 \times \bar{\sigma}_{yy}$	DOF [c]
$N = 4$	3.741	2.544	2.118	1.425	8.461	5.214	2745
$N = 1$	3.749	2.522	−0.053	1.446	5.000	4.870	549
Arlequin [a]	3.729	2.537	2.116	1.424	5.000	5.217	1197
Arlequin [b]	3.716	2.547	−0.056	1.444	8.352	4.807	1197

[a] Refined elements near the loading application zone.
[b] Refined elements near the simply support.
[c] DOF: degrees of freedom.

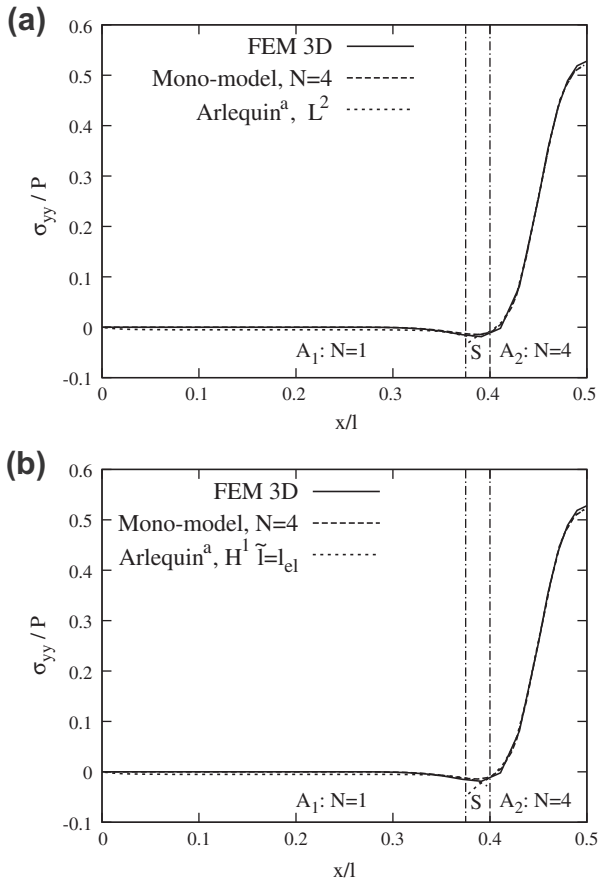

Fig. 8. Dimensionless stress $\bar{\sigma}_{yy}$ along the beam axis for square cross-section, $l/a = 10$, via (a) L^2 coupling and (b) H^1 coupling with $\tilde{l} = l_{el}$.

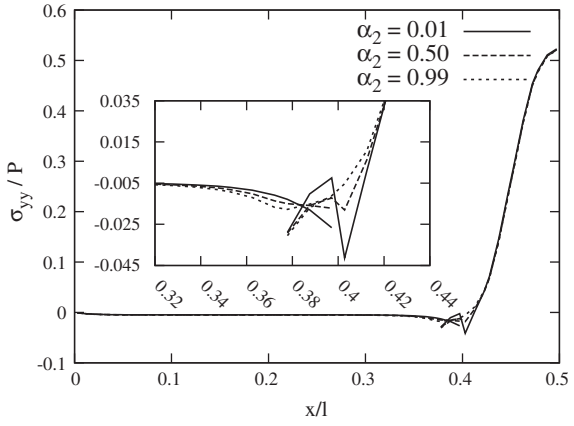

Fig. 9. Dimensionless stress $\bar{\sigma}_{yy}$ along the beam axis varying α_2, square cross-section, $l/a = 10$.

$$\bar{u}_z = \frac{1000 E_T a^3}{l^4 P} u_z \tag{43}$$

$$(\bar{\sigma}_{xx}, \bar{\sigma}_{xz}) = \frac{1}{P}(\sigma_{xx}, \sigma_{xz}) \tag{44}$$

Table 7 shows the results for slender ($l/a = 100$) and deep ($l/a = 10$) beams. Considered theories yield all accurate results for $\bar{u}_z$ in the case of slender beam, whereas deep beam calls for a third-order theory. First- and second-order theories underestimate $\bar{\sigma}_{xz}$ by about 50% with respect to third- and fourth-order models. In the case of deep beam, the normal stress $\bar{\sigma}_{xx}$ computed by high- and low-order

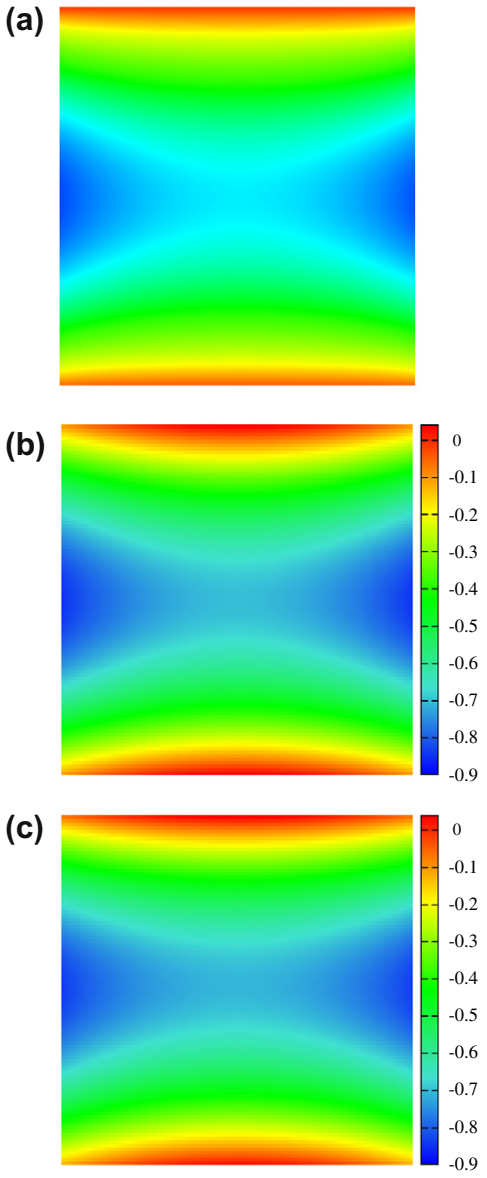

Fig. 10. Dimensionless stress $\bar{\sigma}_{xy}$ above the cross-section at $x = 0$ via (a) FEM 3D solution, (b) fourth-order model and (c) Arlequin-based solution, $l/a = 10$.

theories differ by about 25%. Results computed via the Arlequin method are reported in Table 8. The same coupling as in the previous case has been considered. The value of $\bar{\sigma}_{xz}$ for the configuration addressed as "Arlequin^b" is aligned with that obtained through the fourth-order model, despite the consistent reduction of the number of degrees of freedom. The same consideration holds for $\bar{\sigma}_{xx}$ considering the configuration "Arlequin^a".

6.3. I-shaped cross-section beam

Fig. 12 presents the geometry of the considered I-shaped cross-section, loading and verification points. Beam is made of an isotropic material whose Young's modulus is equal to 75 GPa and whose Poisson's ratio is equal to 0.3. A moderately deep beam $l/a = 30$ is considered. Displacements are put in a dimensionless form according to Eq. (41). Stress components σ_{xx}, σ_{yy}, σ_{zz} and σ_{xy} are normalised towards the loading amplitude P. An expansion order as high as 15 is accounted for. Table 9 shows the displacement components. Results are computed considering 20 elements. They con-

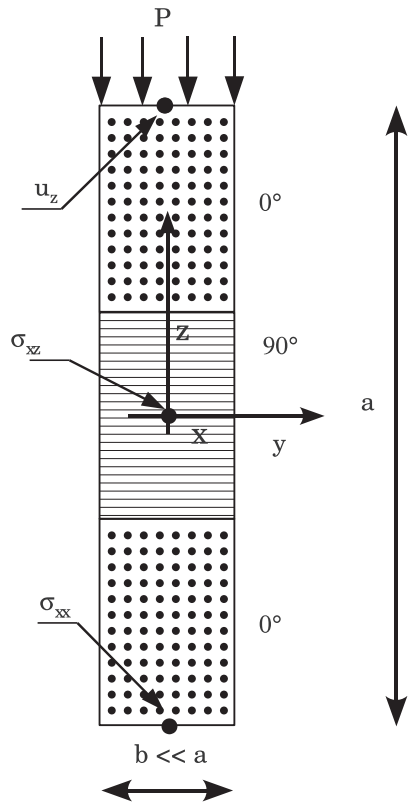

Fig. 11. Cross-section geometry, loading and verification points of cross-ply composite beam.

verge to the analytical solution. Displacement $\bar{u}_x$ is accurately modelled by classical theories. $\bar{u}_y$ predicted via a fourth-order model differs from the reference solution by about 0.3%. Component $\bar{u}_z$ is due to the localised loading and an accurate prediction calls for high-order theories. Fourth-order model underestimates it by about 20%, whereas the difference is about 4% in the case of a 15th-order theory. Dimensionless stresses are reported in Tables 10 and 11. Classical models yield the same value for $\bar{\sigma}^{I}_{xx}$ and $\bar{\sigma}^{II}_{xx}$, being the error about 1.4 and 6%, respectively. σ^{-I}_{xx} is accurately pre-dicted for N as low as three. $\bar{\sigma}^{II}_{xx}$ evaluated via a 15th-order model differs from the reference solution by about 2%. Stress components $\bar{\sigma}_{xy}$, σ^{-}_{zz} and σ^{-}_{yy} call for higher-order models, being the error in the case of a 15th-order theory about 2.2%, 6.2% and 10%, respectively. A more accurate description of normal stress components can be obtained via a localised modelling approach, that is, displacements are approximated in each cross-section subdomain by polynomial functions, such as Lagrange's or Legendre's, that ensure the congru-

Table 8
Mono-theories and variable kinematic models, [0/90/0] beam, $l/a = 10$.

	$10^1 \times \bar{u}_z$	$-10^{-1} \times \bar{\sigma}_{xx}$	$10^1 \times \bar{\sigma}_{xz}$	DOF [c]
$N = 4$	1.898	1.915	4.951	2745
$N = 1$	1.638	1.481	2.499	549
Arlequin [a]	1.668	1.843	2.499	1197
Arlequin [b]	1.720	1.481	5.065	1197

[a] Refined elements near the loading application zone.
[b] Refined elements near the simply support.
[c] DOF: degrees of freedom.

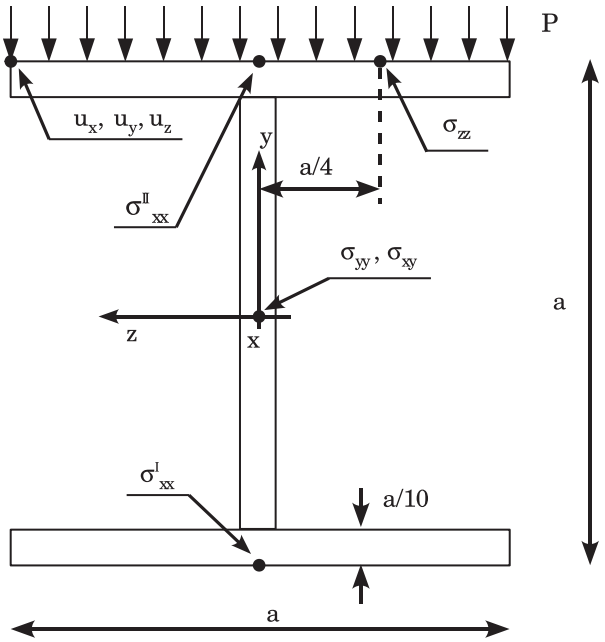

Fig. 12. I-shaped cross-section geometry, loading and verification points.

ency of the displacement fields within sub-domains' shared borders. This will be matter of future investigations. Results computed via the Arlequin method are reported in Table 12. Unless differently stated, the coarse sub-domain A_1 is meshed via 16 sec-ond-order, B4 elements whereas five 15^{th}-order, B4 elements are considered for sub-domain A_2. The Arlequin method proves to be effective in merging sub-domains having different finite elements. The total number of degrees of freedom in the analysis is reduced to less than a third. The variation of $\bar{u}_z$ along the beam axis is pre-sented in Fig. 13. The coupling operators are compared in Fig. 14. Results differ significantly in the superimposed volume and in its neighbourhood increasing $\tilde{l}$, Solutions become coincident moving

Table 7
Dimensionless displacement and stresses for a [0/90/0] beam, $l/a = 100$ and 10.

Analytical UF	$l/a = 100$			$l/a = 10$		
	$\bar{u}_z$	$-10^{-3} \times \bar{\sigma}_{xx}$	$\bar{\sigma}_{xz}$	$\bar{u}_z$	$-10^{-1} \times \bar{\sigma}_{xx}$	$10 \times \bar{\sigma}_{xz}$
$N = 4$	1.040	1.509	5.031	1.898	1.951	5.027
$N = 3$	1.040	1.509	5.004	1.898	1.961	5.025
$N = 2$	1.037	1.500	2.550	1.640	1.417	2.545
$N = 1$	1.038	1.500	2.540	1.642	1.505	2.540
FEM UF B4						
$N = 4$	1.040	1.486	4.952	1.898	1.915	4.951
$N = 3$	1.040	1.486	4.952	1.898	1.930	4.951
$N = 2$	1.037	1.477	2.507	1.640	1.393	2.507
$N = 1$	1.037	1.477	2.499	1.638	1.481	2.499

Table 9
Dimensionless displacements for I-shaped cross-section beam, $l/a = 30$.

	$-\bar{u}_x$			$10^{-1} \times \bar{u}_y$			$-10^2 \times \bar{u}_z$			
FEM 3D	2.082			4.233			5.216			
UF	B2	B3/B4	AS [a]	B2	B3/B4	AS	B2	B3	B4	AS
$N = 15$	2.072	2.073	2.078	4.226	4.231	4.231	5.062	4.987	4.992	4.993
$N = 11$	2.072	2.073	2.078	4.224	4.228	4.228	4.916	4.855	4.859	4.860
$N = 7$	2.072	2.073	2.078	4.219	4.223	4.224	4.532	4.505	4.509	4.509
$N = 4$	2.072	2.073	2.078	4.206	4.211	4.211	4.175	4.177	4.176	4.176
$N = 3$	2.072	2.073	2.078	4.206	4.211	4.211	4.047	4.050	4.050	4.050
$N = 2$	2.072	2.073	2.078	4.169	4.174	4.174	4.002	4.004	4.003	4.003
$N = 1$	2.072	2.072	2.078	4.169	4.174	4.174	0.026	0.024	0.024	0.024
TB	2.073	2.074	2.079	4.169	4.174	4.174	0.000	0.000	0.000	0.000
EB	2.073	2.074	2.079	4.147	4.152	4.152	0.000	0.000	0.000	0.000

[a] Analytical UF solution.

Table 10
Dimensionless stresses $\bar{\sigma}_{xx}$ and $\bar{\sigma}_{xy}$ in the case of beam with I-shaped cross-section, $l/a = 30$.

	$-10^{-2} \times \bar{\sigma}^{I}_{xx}$				$10^{-2} \times \bar{\sigma}^{II}_{xx}$				$10^{-1} \times \bar{\sigma}_{xy}$			
FEM 3D	2.412				2.244				1.769			
UF	B2	B3	B4	AS[a]	B2	B3	B4	AS	B2	B3	B4	AS
$N = 15$	2.390	2.419	2.411	2.411	2.274	2.301	2.294	2.298	1.546	1.787	1.727	1.727
$N = 11$	2.391	2.420	2.412	2.412	2.298	2.325	2.318	2.322	1.636	1.877	1.817	1.817
$N = 7$	2.394	2.422	2.414	2.415	2.331	2.355	2.349	2.351	1.470	1.711	1.651	1.651
$N = 4$	2.375	2.405	2.397	2.397	2.348	2.373	2.367	2.368	1.793	2.034	1.974	1.974
$N = 3$	2.396	2.427	2.419	2.419	2.367	2.394	2.389	2.389	1.793	2.034	1.974	1.974
$N = 2$	2.357	2.384	2.378	2.378	2.354	2.385	2.378	2.378	0.374	0.615	0.555	0.555
$N = 1$	2.371	2.391	2.386	2.386	2.354	2.375	2.370	2.370	0.355	0.595	0.535	0.535
TB	2.362	2.383	2.378	2.378	2.378	2.383	2.378	2.378	0.355	0.595	0.535	0.535
EB	2.362	2.383	2.378	2.378	2.362	2.383	2.378	2.378	–	–	–	–

[a] Analytical UF solution.

Table 11
Dimensionless stresses $\bar{\sigma}_{yy}$ and $\bar{\sigma}_{zz}$ in the case of beam with I-shaped cross-section, $l/a = 30$.

	$-10^{-1} \times \bar{\sigma}_{zz}$				$\bar{\sigma}_{yy}$			
FEM 3D	1.868				5.090			
UF	B2	B3	B4	AS[a]	B2	B3	B4	AS
$N = 15$	2.227	1.938	1.985	1.950	4.801	4.569	4.557	4.565
$N = 11$	2.384	2.061	2.110	2.076	4.146	4.067	4.062	4.073
$N = 7$	1.257	1.096	1.128	1.100	4.471	4.128	4.150	4.156
$N = 4$	0.564	0.467	0.485	0.474	5.111	5.953	5.806	5.771
$N = 3$	0.203	0.084	0.103	0.099	5.704	5.785	5.762	5.738
$N = 2$	0.115	−0.022	0.003	0.002	1.565	1.779	1.785	1.788
$N = 1$	0.046	0.044	0.044	0.044	1.802	1.858	1.865	1.865

[a] Analytical UF solution.

Table 12
Results with the Arlequin method compared to mono-theories models. I-shaped cross-section beam, $l/a = 30$.

	$-\bar{u}_x$	$10^{-1} \times \bar{u}_y$	$-10^2 \times \bar{u}_z$	$10^{-2} \times \bar{\sigma}^{II}_{xx}$	$10^{-1} \times \bar{\sigma}_{xy}$	$\bar{\sigma}_{yy}$	$10^{-1} \times \bar{\sigma}_{zz}$	DOF [c]
$N = 15$	2.073	4.231	4.992	2.294	1.727	4.557	1.985	24,888
$N = 2$	2.073	4.174	4.003	2.378	0.555	1.785	0.003	1098
Arlequin [a]	2.079	4.192	4.990	2.297	0.555	4.563	1.949	7482
Arlequin [b]	2.079	4.188	4.004	2.378	1.725	1.725	0.003	7482

[a] Refined elements near the loading application zone.
[b] Refined elements near the simply support.
[c] DOF: degrees of freedom.

away from the coupling domain. Fig. 15 shows the deformed section at mid-span. The deformed section computed via mono-model 15th-order theory and the variable kinematic model differ mainly by a rigid translation. Arlequin method captures local phenomena such as the absolute value of $^{-}u_z$ and the variation of $^{-}u_y$ along z axis, responsible for the shape of the deformed section. If a quantity in the high-order part of the model strongly depends upon its value in the low-order part where it is not correctly modelled, the inaccuracy propagates from the low- to the high-order part. This is the case of the absolute value of $\bar{u}_y$ that is responsible for the position

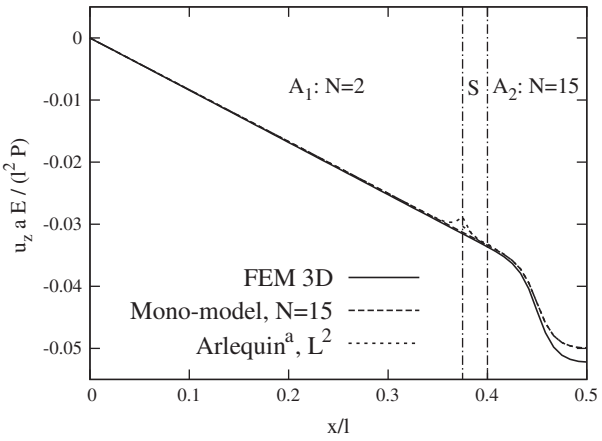

Fig. 13. Dimensionless displacement $\bar{u}_z$ along the axis of the beam, I-shaped cross-section beam, $l/a = 30$, via L^2 coupling.

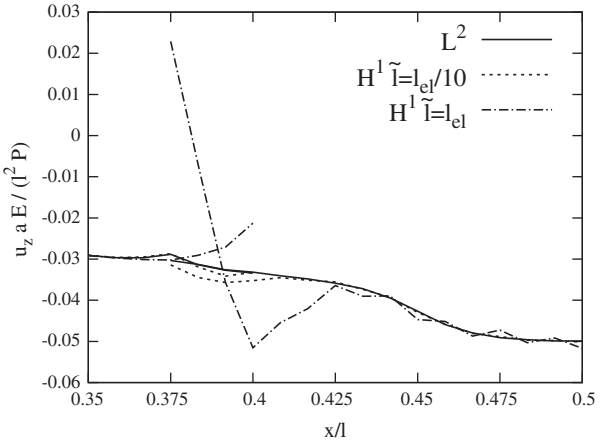

Fig. 14. Coupling operators comparison for dimensionless displacement $\bar{u}_z$ along the axis of the beam, I-shaped cross-section beam, $l/a = 30$.

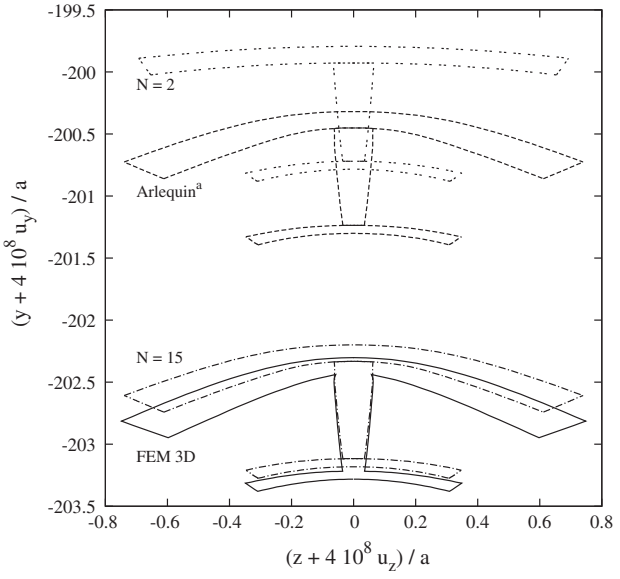

Fig. 15. Deformed cross-section at mid-span in the case of I-shaped cross-section beam, $l/a = 30$.

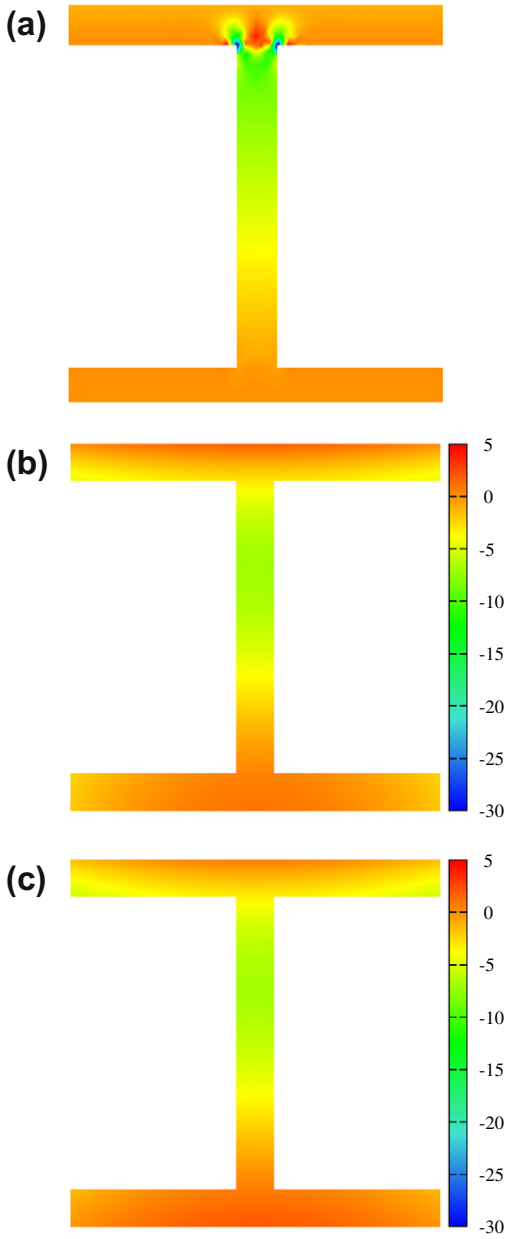

Fig. 16. Dimensionless stress $\bar{\sigma}_{yy}$ above the mid-span cross-section via (a) FEM 3D solution, (b) fourth-order model and (c) Arlequin-based solution linking first- and fourth-order models, $l/a = 30$.

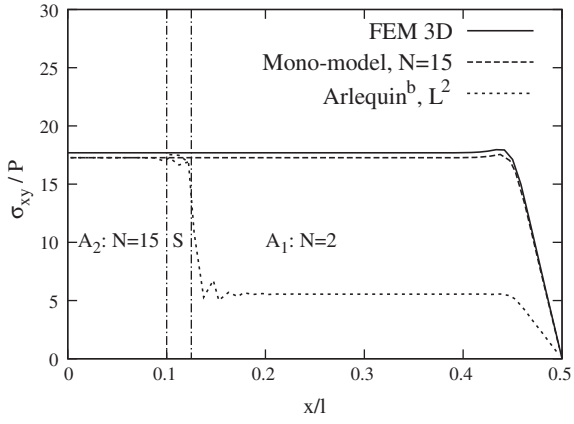

Fig. 17. Dimensionless stress $\bar{\sigma}_{xy}$ along the axis of the beam, I-shaped cross-section beam, $l/a = 30$, via L^2 coupling.

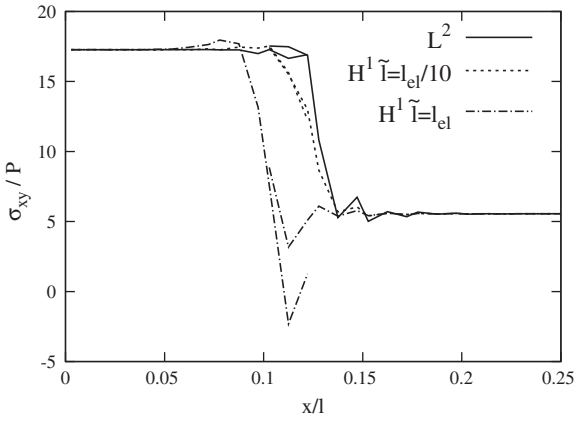

Fig. 18. Coupling operators comparison for dimensionless stress $\bar{\sigma}_{xy}$ along the axis of the beam, I-shaped cross-section beam, $l/a = 30$.

of the deformed section. A qualitatively comparison of the stress component $\bar{\sigma}_{yy}$ among three-dimensional reference solution, fourth-order model with 20 B4 elements and Arlequin-based solution linking first- and fourth-order models is presented in Fig. 16. Beam finite element models are not able to predict stress concentration. Results are in good agreement except near internal corners. Fig. 17 shows the variation of $\bar{\sigma}_{xy}$ along the beam axis. The oscillations in the coupling zone yield small oscillations in its neighbourhood. They depend upon the coupling operator as shown in Fig. 18. H^1 coupling operator yields a smoother solution. Nevertheless, high values of $\tilde{l}$ cause a loss of accuracy.

7. Conclusions

Hierarchical beam finite elements have been used in the context of the Arlequin adaptation method. In order to reduce the computational cost refined finite elements have been employed only in certain sub-domains of the structure where the stress field is quasi-three-dimensional. Hierarchical beam theories are based on a unified formulation that yields the element stiffness matrix in a compact form that does not depend upon the theory approximation order. Higher order models that account for shear deformations and in- and out-of-plane warping can be formulated straightforwardly. Classical models, such as Euler–Bernoulli's and Timoshenko's, are obtained as particular cases. Arlequin coupling matrix has been obtained in the framework of the proposed unified formulation as a fundamental nucleo. Two coupling operators have been accounted for. Proposed results have been validated towards closed form Navier-type solutions and three-dimensional FE models. Square and I-shaped cross-sections have been considered. A cross-ply laminated composite beam is accounted for as well. Slender, moderately deep and deep beams have been investigated. It has been found that the Arlequin method is an effective approach to couple sub-domains of the structure modelled with finite elements having a different expansion order. The size of the superimposition volume has not a significant effect over the quality of the coupling. In order to reduce the computational cost, the coupling volume should be discretised via only a finite element. The expression of the coupling matrix in terms of its fundamental nucleo guarantees a straightforward implementation of the Arlequin method. Theory approximation order can be considered as a free parameter. Accurate results have been obtained in the high-order part of the model with a significant reduction of the total number of degrees of freedom.

Acknowledgements

First author acknowledges the financial support by Fonds National de la Recherche of Luxembourg under AFR Grants PHD-08-069. Part of the work of the second author is supported by the FNR Project CORE 2009 C09/MS/05 FUNCTIONALLY. Last two authors acknowledge the AM2c mobility support by Fonds National de la Recherche of Luxembourg. Dr. Hu acknowledges also the National Natural Science Foundation of China (Grant No. 10802059).

References

[1] Timoshenko SP. On the corrections for shear of the differential equation for transverse vibrations of prismatic bars. Philos Mag 1921;41:744–6.
[2] Timoshenko SP. On the transverse vibrations of bars of uniform cross section. Philos Mag 1922;43:125–31.
[3] Saint-Venant B. Memoire Sur la Torsion des Prismes. Mem Savants Etrangers 1855;14:233–560.
[4] Prandtl L. Zur Torsion von Prismatischen Stäben. Z Physik 1903;4:758–70.
[5] Kapania RK, Raciti S. Recent advances in analysis of laminated beams and plates, part i: shear effects and buckling. AIAA J 1989;27(7):923–34.
[6] Kapania RK, Raciti S. Recent advances in analysis of laminated beams and plates, part ii: vibrations and wave propagation. AIAA J 1989;27(7):935–46.
[7] Hodges DH. A review of composite rotor blade modeling. AIAA J 1990;28(3):561–5.
[8] Jung SN, Nagaraj VV, Chopra I. Assessment of composite rotor modeling techniques. J Am Helicopter Soc 1999;44(3):188–205.
[9] Carrera E, Giunta G. Refined beam theories based on a unified formulation. Int J Appl Mech 2010;2(1):117–43.
[10] Carrera E, Giunta G, Nali P, Petrolo M. Refined beam elements with arbitrary cross-section geometries. Comput Struct 2010;88(5–6):283–93.
[11] Bank RE. Adaptive computational methods for partial differential equations. Philadelphia: SIAM; 1983.
[12] Szabo BA, Babuska I. Finite element analysis. John Wiley & Sons; 1991.
[13] Bathe KJ. Finite element procedure. Prentice Hall; 1996.
[14] Fish J, Pan L, Belsky V, Gomaa S. Unstructured multigrid method for shells. Int J Numer Methods Eng 1996;39(7):1181–97.
[15] Möes N, Dolbow J, Belytschko T. A finite element method for crack growth without remeshing. Int J Numer Methods Eng 1999;46(1):131–50.
[16] Fish J. The s-version of the finite element method. Comput Struct 1992;43(3):539–47.
[17] Fish J, Markolefas S. Adaptive s-method for linear elastostatics. Comput Methods Appl Mech Eng 1993;103:363–96.
[18] Blanco PJ, Feijoo RA, Urquiza SA. A variational approach for coupling kinematically incompatible structural models. Comput Methods Appl Mech Eng 2008;197:1577–620.
[19] Ben Dhia H. Multiscale mechanical problems: the Arlequin method. C R Acad Sci Ser IIB Mech Phys Astron 1998;326(12):899–904.
[20] Ben Dhia H. Numerical modelling of multiscale problems: the Arlequin method. In: CD Proceedings ECCM'99, Munchen; 1999.
[21] Ben Dhia H, Rateau G. The Arlequin method as a flexible engineering tool. Int J Numer Methods Eng 2005;62(11):1442–62.
[22] Hu H, Belouettar S, Potier-Ferry M, Daya EM. Multi-scale modelling of sandwich structures using the Arlequin method part i: linear modelling. Finite Elements Anal Des 2008;45(1):37–51.
[23] Hu H, Belouettar S, Potier-Ferry M, Daya EM, Makradi A. Multi-scale nonlinear modelling of sandwich structures using the Arlequin method. Compos Struct 2010;92(2):515–22.
[24] Reddy JN. Mechanics of laminated composite plates and shells. Theory and analysis. CRC Press; 2004.
[25] Carrera E, Brischetto S. Analysis of thickness locking in classical, refined and mixed multilayered plate theories. Compos Struct 2008;82(4):549–62.
[26] Carrera E, Brischetto S. Analysis of thickness locking in classical, refined and mixed theories for layered shells. Compos Struct 2008;85(1):83–90.
[27] Abaqus theory manual, version 6.5. Hibbit and Karlson and Sorensen Inc.; 2005.